

Suppressed Quenching of Purcell-Enhanced Single-Molecule Emission in Plasmonic Nanocavities

Nuttawut Kongsuwan,¹ Angela Demetriadou,¹ Rohit Chikkaraddy,² Felix Benz,² Vladimir A. Turek,² Ulrich F. Keyser,² Jeremy J. Baumberg,² and Ortwin Hess¹

¹*Blackett Laboratory, Prince Consort Road, Imperial College London, London SW7 2AZ, UK*

²*Cavendish Laboratory, University of Cambridge, Cambridge CB3 0HE, UK*

(Dated: June 19, 2022)

An emitter in the vicinity of a metal nanostructure is quenched by its dominant decay through non-radiative channels. This has led to the strong belief in a zone of inactivity for emitters placed $<10\text{nm}$ from a plasmonic nanostructure. We demonstrate this quenching is strongly suppressed for tightly-coupled plasmonic resonators that form nanocavities, due to plasmon mixing which completely alters the behaviour of the overall system. Compared to an isolated spherical nanoparticle, the decay channels of a nanocavity show mode hybridization which massively enhances emitter excitation and decay via radiative channels. This creates ideal conditions for realizing single-molecule strong-coupling with plasmons, evident in semi-classical calculations. Experimentally we find quenching is indeed absent in plasmonic nanocavities.

The lifetime of an excited atomic state is determined by the inherent properties of the atom and its environment, first reported by Purcell [1], and experimentally verified by placing an atomic emitter within various optical geometries [2–4]. Plasmonic structures have the ability to massively enhance electromagnetic fields, and therefore dramatically alter the excitation rate of an emitter [5]. However, it is well known that placing an emitter close to a plasmonic structure ($<10\text{nm}$), quenches its fluorescence [6–8]. Analysis by Anger et al. [5] showed this is due to the coupling of the emitter to non-radiative higher-order plasmonic modes that dissipate its energy. This ‘zone of inactivity’ is believed to quench all quantum emitters.

Recently we reported light-matter strong-coupling of a single-molecule placed within a plasmonic nanocavity [9]. Such nanocavities are formed by two plasmonic (metal) structures separated by just a few nanometers. In these experiments, a nanoparticle-on-mirror (NPoM) geometry is used, where a gold nanoparticle is assembled onto a gold surface with an emitter placed within the sub-nm (0.9nm) gap. Clearly, the emitter is within the quenching regime of both the nanoparticle and the mirror, and one might assume that this single emitter should be dark and never strongly-couple to plasmons. However, when two plasmonic structures are brought close together forming a cavity: (i) the decay channels of the system change, (ii) the main mode that an emitter couples to alters, and (iii) higher-order modes are not necessary non-radiative and dissipative [10–14].

In this Letter, we demonstrate that quenching is suppressed in plasmonic nanocavities, due to a dramatic increase of both the emitter excitation and decay rates into radiative channels. Modes in plasmonic nanocavities are not a simple superposition of modes of the isolated structures, but hybrid-plasmonic states [15–19]. Hence, higher-order modes that are dark for an isolated spherical nanoparticle, radiate efficiently for tightly-coupled

plasmonic structures [11], significantly reducing the non-radiative decay and quenching. By comparing an isolated nanoparticle with a NPoM nanocavity, we quantify their different radiative and non-radiative channels, explaining the mechanism that leads to suppression of quenching in plasmonic nanocavities. We note very similar results to the NPoM are obtained with a nanoparticle dimer. With semi-classical Maxwell-Bloch descriptions of a two-level emitter, we perform Finite-Difference Time-Domain (FDTD) calculations, giving the emission dynamics in each system. Finally, using DNA-origami to control the position of a single emitter in the nanogap, we experimentally demonstrate the suppression of quenching in plasmonic nanocavities.

The fluorescence/emission rate γ_{em} of an emitter depends on its excitation rate (γ_{exc}), and its radiative decay rate (i.e. quantum yield, $\eta = \gamma_{\text{rad}}/\gamma_{\text{tot}}$) as [5]:

$$\gamma_{\text{em}} = \gamma_{\text{exc}} \eta = \gamma_{\text{exc}} \left(\frac{\gamma_{\text{rad}}}{\gamma_{\text{tot}}} \right) \quad (1)$$

where γ_{rad} and γ_{tot} are the radiative and total (Purcell factor) decay rates of the emitter. The normalized excitation rate is governed by the field enhancement at the position of the emitter, and assuming that the environment does not affect the emitter’s polarizability:

$$\tilde{\gamma}_{\text{exc}} = \frac{\gamma_{\text{exc}}}{\gamma_{\text{exc}}^0} = \left| \frac{\hat{\mathbf{p}} \cdot \mathbf{E}(\mathbf{r}=0)}{\hat{\mathbf{p}} \cdot \mathbf{E}_0(\mathbf{r}=0)} \right|^2 \quad (2)$$

where $\hat{\mathbf{p}}$ is the emitter’s polarizability unit vector, $\mathbf{E}(\mathbf{r}=0)$ is the total (incident and scattered) electric field and $\mathbf{E}_0(\mathbf{r}=0)$ the incident field at $\mathbf{r}=0$ where the emitter is placed. The quantum yield of an emitter with radiative decay rate $\gamma_{\text{rad}} = \gamma_{\text{tot}} - \gamma_{\text{nr}}$ is calculated assuming that non-radiative decay is due to the Ohmic losses of the metal [5]: $\gamma_{\text{nr}} \propto \int_V \text{Re}\{\mathbf{j}(\mathbf{r}) \cdot \mathbf{E}_m^*(\mathbf{r})\} d\mathbf{r}^3$.

In the case of an isolated spherical nanoparticle, an emitter couples dominantly to the nanoparticle dipolar

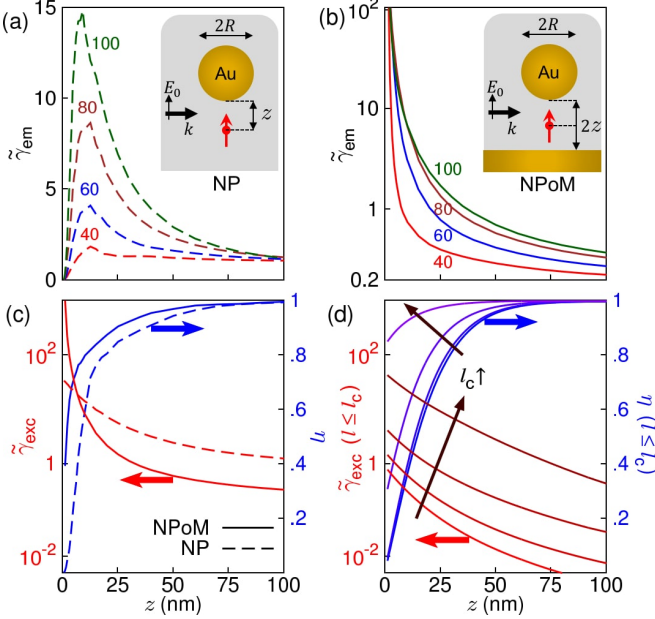


FIG. 1. Fluorescence rate $\tilde{\gamma}_{\text{em}}$ of an emitter with transition $\lambda=650\text{nm}$ placed at distance z from (a) an isolated nanoparticle and (b) inside the NPoM nanocavity, for sphere diameters $2R=40,60,80,100\text{nm}$ and with background permittivity $\epsilon_D=1.96$. (c) The excitation rate $\tilde{\gamma}_{\text{exc}}$ (red) and quantum yield η (blue) for an isolated nanoparticle (dotted lines) and a nanocavity (solid lines) of nanoparticle diameter 80nm . (d) Coupling contributions to the excitation rate (red) and quantum yield (blue) when truncating the hybridization terms at $l_c = 2, 3, 5$ and 10 .

(first-order) mode. However as the emitter approaches the nanoparticle, it couples increasingly to higher-order modes, which are dark. This leads to its energy dissipation via Ohmic losses (quenching). Figure 1(a) shows the normalized fluorescence rate $\tilde{\gamma}_{\text{em}} = \eta \tilde{\gamma}_{\text{exc}}$ for an isolated nanoparticle, calculated for a classical dipole approach-

ing the structure, using FDTD simulations. Quenching appears when the emitter is placed at $z < 10\text{nm}$, in line with previously reported results [5]. By contrast, similar calculations for the NPoM nanocavity with the emitter always in the center of the nanocavity [Fig. 1(b)] reveal that the emission rate increases by several orders of magnitude (note log scale). As z decreases, the gap between nanoparticle and mirror reduces, and both plasmonic surfaces approach the emitter, but $\tilde{\gamma}_{\text{em}}$ exponentially increases. Since the emission rate is a product of the excitation and radiative rates, we plot them separately [Fig. 1(c)] for both an isolated nanoparticle (dashed lines) and the nanocavity (solid lines). As the emitter is progressively confined within the nanocavity, its excitation rate exponentially increases, due to the very high confinement of the plasmon modes within the gap. Additionally, the quantum yield (η) of the nanocavity out-performs the isolated nanoparticle by more than an order of magnitude as the gap decreases. While non-local effects can affect the actual rates for emission, excitation, and quantum yield of both structures at sub-nm spacings, no significant impact is expected on this qualitative behaviour [20].

To demonstrate the origin of these different behaviours, we adapt the analytical description of [15, 16] for coupled plasmon modes. Isolated spherical nanoparticle follow Mie theory, but the problem of two coupled plasmonic nanoparticles is analytically more complex. It has been solved in the quasi-static limit using several techniques, such as transformation optics [21–23] and multipole expansion [17–19, 24]. However, here the formalism of [15, 16] is more appropriate since it accounts for the coupling of the bare modes of the two plasmonic structures. Adapting this description for the NPoM (by approximating the mirror as a large sphere of radius $r_m=1\mu\text{m}$), the field enhancement in the middle of the nanocavity gap is given by [15]:

$$E(r=0)/E_0 \simeq \alpha^{\text{NP}} \left(\frac{R}{R+z} \right)^3 + \alpha^m \left[1 + \sum_{l=2}^{\infty} \frac{\sqrt{\omega_1 \omega_l}}{\omega_l - \omega - i\gamma/2} \left(\frac{l+1}{2} \right)^2 \frac{R^{(2l+1)}}{(R+z)^{(l+2)} r_m^{l-1}} \right] \quad (3)$$

where R is the radius of the nanoparticle, $2z$ is the gap size assuming the emitter is in the middle of the gap, and $\omega_l = \omega_p \sqrt{l/(2l+1)}$ is the resonant frequency of mode l , with ω_p and γ the metal plasmon frequency and damping. The nanoparticle polarizability $\alpha^{\text{NP}} = 2 \frac{(\epsilon_{\text{Au}}-1)}{(\epsilon_{\text{Au}}+1)}$, while the mirror polarizability α^m is given by Mie scattering (beyond the quasi-static limit) in [25]. The first term provides the field enhancement contribution of the nanoparticle dipole mode, the first term in square brackets is the mirror dipole mode, and the second term in square brackets is the coupling of the mirror to the higher-order

modes of the nanoparticle ($l \geq 2$). In Figure 1(d) we plot this latter contribution of the coupling terms in equation (3) to the excitation rate (red lines) while truncating at increasingly high-order modes. As the nanocavity gets smaller ($z \downarrow$), higher-order mode hybridization is needed to account for the exponential increase of the NPoM excitation rate (seen in Fig. 1c). Similarly, the quantum yield increases with increasingly higher-order hybridization between the two structures. Both these demonstrate that the mode hybridization of the coupled plasmonic structures forming the nanocavity alter the fluorescence rate

of an emitter in a way that fully compensates quenching.

The spectral dependence of the radiative, total, and excitation rates for both the isolated nanoparticle and the nanocavity, varying the nanoparticle diameter from 20nm to 100nm, show strongly contrasting behaviour (Fig. 2). Again the emitter is 0.5nm from the Au surfaces, or at the centre of the 1nm gap. Isolated quasi-static nanoparticles (with $2R < 100$ nm) possess diameter-independent modes [Fig. 2(a,c,e)]. However the resonant wavelengths of the nanocavity modes are highly dependent on the system geometry [11, 26] [Fig. 2(b,d,f)]. The NPoM radiative decay rate $\tilde{\gamma}_{\text{rad}} = \gamma_{\text{rad}}/\gamma_0$, normalized to the free space decay rate γ_0 , is three orders of magnitude larger than for the isolated nanoparticle, with the NPoM dipole ($l = 1$) mode significantly red-shifting for larger NPs. Additionally the quadrupole NPoM mode ($l = 2$) strongly radiates and for larger nanoparticles has comparable radiative rates to the dipole ($l = 1$) mode, in great contrast with the isolated nanoparticle. These large $\tilde{\gamma}_{\text{rad}}$ suppress quenching, and allow strong-coupling dynamics to be radiated into the far-field.

The Purcell factor (normalized total decay rate $\tilde{\gamma}_{\text{tot}} = \gamma_{\text{tot}}/\gamma_0$) for both plasmonic structures shows a diameter-independent broad peak at $\lambda_{\text{pm}} \simeq 550$ nm [Fig. 2(c,d)], which corresponds to the superposition of multiple high-order plasmonic modes, recently referred to as a ‘pseudomode’ [21, 27]. However, the negligible $\tilde{\gamma}_{\text{rad}}$ at λ_{pm} shows the large $\tilde{\gamma}_{\text{tot}}$ comes from emission coupled to the pseudo-mode decaying via non-radiative channels ($\tilde{\gamma}_{\text{tot}} = \tilde{\gamma}_{\text{rad}} + \tilde{\gamma}_{\text{nr}}$). In contrast to recent proposals [21], this suggests the nanocavity pseudo-mode quenches emission almost entirely via non-radiative channels, as it does for isolated nanoparticles, suppressing any way to observe possible strong-coupling dynamics. At the NPoM dipole and quadrupole resonant wavelengths, $\tilde{\gamma}_{\text{rad}} \sim \tilde{\gamma}_{\text{tot}}/2$. Hence, during coherent energy exchange between the emitter and the dipole/quadrupole modes, far-field radiation is imprinted with any Rabi-oscillations allowing tracking of these hybrid states.

Additionally, the excitation rate $\tilde{\gamma}_{\text{exc}}$ of an emitter next to an isolated nanoparticle is two orders of magnitude smaller than for a 1nm nanocavity [Fig. 2(e,f)]. Hence for an isolated nanoparticle where $\tilde{\gamma}_{\text{rad}} \ll \tilde{\gamma}_{\text{tot}}$, an emitter is weakly excited and heavily quenched by the pseudomode. On the other hand, the NPoM nanocavity strongly excites the emitter for dipole/quadrupole modes, with $\tilde{\gamma}_{\text{exc}}$ increasing for larger nanoparticles. Since $\tilde{\gamma}_{\text{rad}} \sim \tilde{\gamma}_{\text{tot}}/2$, there is significant energy both radiated and exchanged between emitter and plasmons, allowing us to measure strong-coupling dynamics at room temperature. This difference between the two systems is why room-temperature strong coupling of a single emitter in a plasmonic nanocavity is reached, and can also be measured [9], but not with an isolated plasmonic structure.

While the classical calculations presented so far pro-

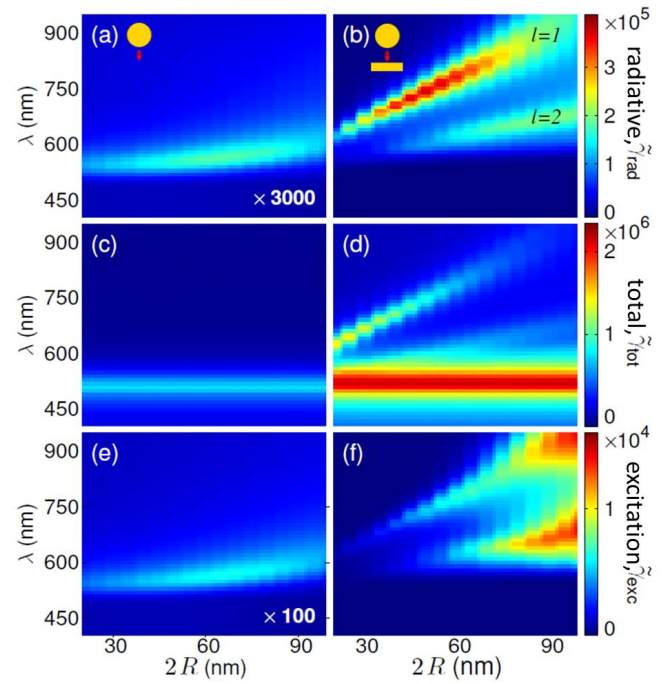


FIG. 2. Spectra for a vertically-oriented emitter placed (a,c,e) 0.5nm below an isolated nanoparticle, and (b,d,f) inside a 1nm-wide NPoM nanocavity. (a,b) Normalized radiative decay rate $\tilde{\gamma}_{\text{r}}$, (c,d) Normalized total decay rate $\tilde{\gamma}_{\text{tot}}$ (Purcell factor), and (e,f) Normalized excitation rate $\tilde{\gamma}_{\text{exc}}$.

vide useful insights into the radiative and non-radiative decay channels of these differing plasmonic systems, they cannot reveal the temporal-dynamics of an emitter coupling to the plasmons. We thus now use a two-level Maxwell-Bloch description [28] for the emitter, where the excited- (N_2) and ground- (N_1) state populations are described by:

$$\frac{\partial N_2}{\partial t} = -\frac{\partial N_1}{\partial t} = -\gamma N_2 + \frac{1}{\hbar\omega_0} \left(\frac{\partial \mathbf{P}}{\partial t} + \Gamma \mathbf{P} \right) \cdot \mathbf{E} \quad (4)$$

where \mathbf{E} is the local field exciting the emitter, \mathbf{P} the induced macroscopic polarizability, $\omega_0 = 2\pi/\lambda$ the transition frequency, and $\gamma=0.66\mu\text{eV}$ and $\Gamma=28\text{meV}$ are the relaxation and dephasing rates of the emitter. The E_z -field time evolution after broadband pulsed excitation without an emitter (red) is modified with a two-level emitter (blue) placed a distance of 0.5nm from the isolated nanoparticle of diameter 40nm or in the middle of the 1nm nanocavity [Fig. 3(a,b)]. In both cases, the emitter absorbs energy from the plasmons, with the excited state population (N_2 , relative to value at 100fs for the NPoM, black dashed line) peaking at ~ 25 fs. This excited population decays, re-emitting part of the absorbed energy in both plasmonic systems. However, only in the nanocavity does re-emission lead to further plasmon re-excitation after ~ 30 fs (i.e. Rabi-oscillation). To demonstrate the different strong-coupling strengths as an emit-

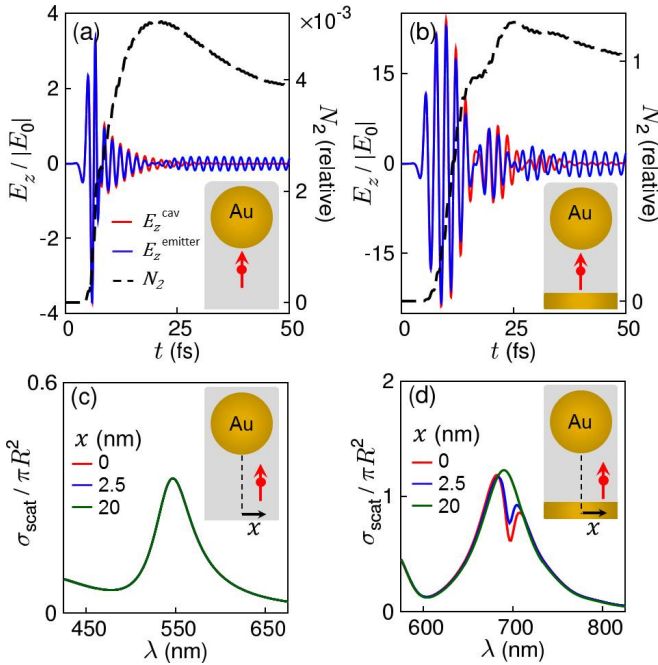


FIG. 3. Temporal E_z dynamics for (a) isolated nanoparticle and (b) 1nm-wide NPoM without (red) and with (blue) the presence of a two-level emitter 0.5nm below the nanoparticle of diameter 40nm. (c,d) Corresponding scattering cross-sections for (c) isolated nanoparticle and (d) NPoM, with the two-level quantum emitter placed laterally at $x=0$, 2.5, and 20nm. Emitter transitions are at $\lambda = 550$ and 700nm tuned to the dipole mode of each system.

ter approaches an isolated nanoparticle or a plasmonic nanocavity, we plot the scattering cross-sections for an emitter placed at $z = 0.5$ nm and lateral positions $x=0$, 2.5, and 20nm [Fig. 3(c,d)]. Scattering spectra of an isolated nanoparticle show no dependence on the emitter position, while for the NPoM nanocavity the characteristic Rabi-splitting is observed only when the emitter is well within the nanocavity.

Tuning the gap width shifts the resonant mode making experimental implementations with a resonant emitter difficult. Hence to highlight the differences in quenching, we shift the emitter laterally inside a fixed gap. Simulations [Fig. 4(a)] show the dependence of the excited state population N_2 at time 100fs (after the emitter has relaxed through dephasing) for different lateral placements, x . For the isolated nanoparticle (blue line), N_2 quenches for $x < 5$ nm and is three orders of magnitude smaller than for the NPoM (red line) which is instead enhanced for $x < 5$ nm.

We compare with experiments placing a single Cy5 molecule within NPoM nanocavities formed by 80nm diameter nanoparticles. DNA-origami [29] is used to create a 5nm-thick spacer to control the emitter position with sub-nm lateral and vertical accuracy relative to the gold-nanoparticle [Fig. 4(b) inset]. We illuminate the

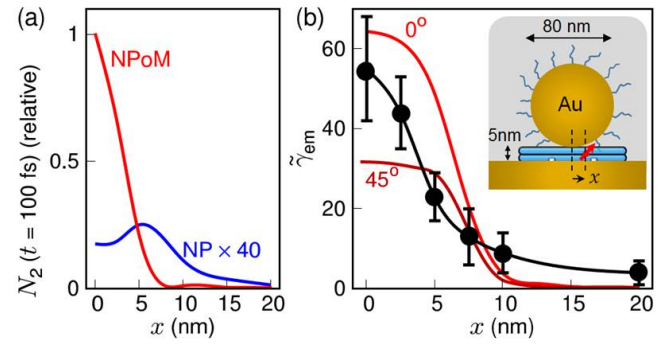


FIG. 4. (a) Excitation efficiency of a two-level emitter vs lateral position next to an isolated nanoparticle diameter 40nm or 1nm-wide NPoM. (b) Experimental (black) and numerical (red) emission intensities of a single Cy5 molecule inside a DNA-origami structure with 5nm nanocavity gap and 80nm diameter. Molecule is horizontally displaced by x from center of nanocavity and excited by a 633nm laser.

nanocavity with a high numerical aperture (NA = 0.8) objective, filling the back focal plane of the aperture with 633nm laser light. In simulations this is suitably modelled by two out-of-phase sources incident from either side of the NPoM at 55° angle of incidence (inset). The experimental emission rates at different lateral positions [Fig. 4(b),black points] quantitatively match the numerically-calculated emission rates for dipoles oriented along the z -axis and at 45°, as indicated. Different DNA-origami foldings result in slightly different dipole orientations. Partial melting of the double-stranded DNA and uncertainty in the nanoparticle placement yield the uncertainty in emitter position. These small variations lead to different emission intensities in different NPoMs, shown as vertical error bars in the experimental data [Fig 4(b)]. It is evident that an emitter in a plasmonic nanocavity does not quench when placed in the vicinity (< 10 nm) of metal particles, but instead its emission rate enhances when moved towards the center of the nanocavity.

In conclusion, we have demonstrated analytically, numerically, and experimentally that an emitter placed within a plasmonic nanocavity does not quench, despite being in close proximity to a metal nanoparticle. This is due to the radiative nature of higher-order modes in plasmonic nanocavities, which do not lead to non-radiative dissipation but in fact facilitate the re-emission of its energy. Plasmonic nanocavities do not quench emitters, but actually provide the necessary conditions to achieve and observe single-molecule strong-coupling with plasmons at room temperature, and many other related light-matter interactions. Nanocavities are fundamentally different to isolated nanoparticles.

We acknowledge support from EPSRC grants EP/G060649/1 and EP/L027151/1 and European Research Council grant LINASS 320503. N.K. and A.D.

contributed equally to this work.

[1] E. Purcell, *Physical Review* **69**, 681 (1946).

[2] K. Drexhage, *Progress in Optics* **12**, 163 (1974).

[3] D. Kleppner, *Physical Review Letters* **47**, 233 (1981).

[4] P. Lodahl, A. F. van Driel, I. S. Nikolaeva, A. Irman, K. Overgaag, D. Vanmaekelbergh, and W. L. Vos, *Nature* **430**, 654 (2004).

[5] P. Anger, P. Bharadwaj, and L. Novotny, *Physical Review Letters* **96**, 113002 (2006).

[6] E. Dulkeith, A. C. Morteani, T. Niedereichholz, T. A. Klar, J. Feldmann, S. A. Levi, F. C. J. M. van Veggel, D. N. Reinhoudt, M. Mller, and D. I. Gittins, *Physical Review Letters* **89**, 203002 (2002).

[7] S. Kuhn, U. Hakanson, L. Rogobete, and V. Sandoghdar, *Physical Review Letters* **97**, 017402 (2006).

[8] C. M. Galloway, P. G. Etchegoin, and E. C. L. Ru, *Physical Review Letters* **103**, 063003 (2009).

[9] R. Chikkaraddy, B. de Nijs, F. Benz, S. J. Barrow, O. A. Scherman, E. Rosta, A. Demetriadou, P. Fox, O. Hess, and J. J. Baumberg, *Nature* **535**, 127 (2016).

[10] Y. C. Jun, R. D. Kekatpure, J. S. White, and M. L. Brongersma, *Physical Review B* **78**, 153111 (2008).

[11] J. Mertens, A. Demetriadou, R. W. Bowman, F. Benz, M. E. Kleemann, C. Tserkezis, Y. Shi, H. Y. Yang, O. Hess, J. Aizpurua, and J. J. Baumberg, *Nano Letters* **16**, 5605 (2016).

[12] R. Faggiani, J. Yang, and P. Lalanne, *ACS Photonics* **2**, 1739 (2015).

[13] J. Yang, J.-P. Hugonin, and P. Lalanne, *ACS Photonics* **3**, 395 (2016).

[14] J. Yang, R. Faggiani, and P. Lalanne, *Nanoscale Horizons* **1**, 11 (2016).

[15] G. Sun and J. Khurgin, *Applied Physics Letters* **97**, 263110 (2010).

[16] G. Sun and J. Khurgin, *Applied Physics Letters* **98**, 113116 (2011).

[17] S. J. Norton and T. Vo-Dinh, *Journal of Optical Society of America A* **25**, 2767 (2008).

[18] A. Dhawan, S. J. Norton, M. D. Gerhold, and T. Vo-Dinh, *Optics Express* **17**, 9688 (2009).

[19] T. Vo-Dinh, A. Dhawan, S. J. Norton, C. G. Khoury, H.-N. Wang, V. Misra, and M. D. Gerhold, *Journal of Physical Chemistry C* **114**, 7480 (2010).

[20] C. Tserkezis, N. Stefanou, M. Wubs, and N. A. Mortensen, *Nanoscale* **8**, 17532 (2016).

[21] R.-Q. Li, D. Hernangomez-Perez, F. Garcia-Vidal, and A. Fernandez-Dominguez, *Physical Review Letters* **117**, 107401 (2016).

[22] R. Zhao, Y. Luo, A. I. Fernandez-Dominguez, and J. B. Pendry, *Physical Review Letters* **111**, 033602 (2013).

[23] Y. Luo, R. Zhao, and J. B. Pendry, *Proceedings of the National Academy of Sciences* **111**, 18422 (2014).

[24] F. G. de Abajo, *Physical Review B* **60**, 6086 (1999).

[25] H. Kuwata, H. Tamari, K. Esumi, and K. Miyano, *Applied Physics Letters* **83**, 4625 (2003).

[26] C. Tserkezis, R. Esteban, D. O. Sigle, J. Mertens, L. O. Herrmann, J. J. Baumberg, and J. Aizpurua, *Physical Review A* **92**, 053811 (2015).

[27] A. Delga, J. Feist, J. Bravo-Abad, and F. J. Garcia-Vidal, *Physical Review Letters* **112**, 253601 (2014).

[28] R. W. Boyd, *Non-linear Optics* (Elsevier, United States of America, 2008).

[29] V. V. Thacker, L. O. Herrmann, D. O. Sigle, T. Zhang, T. Liedl, J. J. Baumberg, and U. F. Keyser, *Nature Communications* **5**, 3448 (2014).